Ecological Indicators 154 (2023) 110847

Contents lists available at ScienceDirect

Ecological Indicators

journal homepage: www.elsevier.com/locate/ecolind

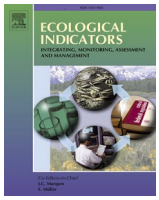

Effects of water masses on the zooplankton community structure in the northern East China Sea during the East Asian Summer Monsoon in 2020

Seohwi Choo [a], Myeong-Taek Kwak [b], Yang-Ki Cho [c], Yang Ho Yoon [d], Ho Young Soh [a,b,d,*]

[a] Big Data Fishery Resource Management Interdisciplinary Program, Chonnam National University, Yeosu, South Korea
[b] Fishery Resource Management Research Institute based on ICT, Chonnam National University, Yeosu, South Korea
[c] School of Earth and Environmental Sciences/Research Institute of Oceanography, Seoul National University, Seoul, South Korea
[d] Department of Ocean Integrated Science, Chonnam National University, Yeosu, South Korea

ARTICLE INFO

Keywords:
Indicator species
MOCNESS
Northern East China Sea
Zooplankton community
Stratified sampling

ABSTRACT

The prolonged rainy season in 2020 was classified as the second-largest rainfall event since 1961. In this study, we conducted a survey to assess fluctuations in the zooplankton community structure of the northern East China Sea (nECS) after the rainy season in August 2020. We examined 24 stations and observed several environmental factors, including water temperature, salinity, chlorophyll-*a* concentration, suspended particulate matter (SPM), and phytoplankton density. Zooplankton samples were collected from 12 stations using MOCNESS to target the surface mixed layer (SML), pycnocline layer (PNC), and lower layer (LL). In regions with low water temperatures, the Yellow Sea and northern East China Sea shelf mixed water community in each layer exhibited a decrease in the relative abundance of *Calanus sinicus*, whereas the incidence of *Paracalanus parvus* s. l. showed an increasing trend. Similarly, in areas with low salinity, the CDW and northern East China Sea shelf mixed water community in SML and PNC displayed comparable distributions, with a tendency for the relative abundance of *Acartia pacifica* and *Paracalanus parvus* s. l. to show a replacement pattern. Moreover, the Tsushima Warm Current (TWC) community in each layer, characterized by high water temperature and salinity, showed a high relative abundance of *Oncaea* spp. and a diverse species distribution, mainly in the eastern part of the study area. Our study identified multiple vertically distributed communities, providing detailed information on water mass structures through cluster analysis. This approach enhanced previous studies by offering novel insights into the vertical structure of water masses and their association with zooplankton communities in the nECS.

1. Introduction

The structure of zooplankton communities can provide key insights into the biological or non-biological interactions that occur in their surrounding pelagic ecosystem, making zooplankton a crucial indicator of marine environments (Landry et al., 2020; Shin et al., 2022). Additionally, zooplankton serves as an important regulator in maintaining the biochemical balance within marine ecosystems, as their short life cycles and high sensitivity to environmental changes provide serve as an indirect indicator of the variations in marine ecosystems (Taylor et al., 2002; Hays et al., 2005). Therefore, understanding zooplankton assemblages is of great significance in comprehending the dynamics of fluctuating marine ecosystems. In line with recent research trends, indicator species analysis (IndVal) has been proposed as a promising means to assess marine ecosystems by extracting indicator species from the zooplankton community (Tseng et al., 2008; Shi et al., 2018; Jeong et al., 2022). This analysis facilitates the identification of associations between specific assemblages and environmental conditions, providing a deeper understanding of the ecological dynamics and responses to environmental changes within the study area.

The northern East China Sea (nECS) borders China to the west, Japan to the east, and Jeju Island of Korea to the north. The nECS has an average depth of approximately 120 m, with depths increasing from west to east. The environmental conditions in the nECS are influenced by the Taiwan Warm Current (TWWC), Kuroshio Current (KC), Tsushima Warm Current (TSWC), and Changjiang diluted water (CDW), resulting in complex spatiotemporal variations in water mass structures (Cho et al., 2009; Lie and Cho, 2016; Liu et al., 2021). These currents play a crucial role in transporting oceanic materials, heat, and salinity, forming a constant front all year round (Hickox et al., 2000; Park and

* Corresponding author at: Big Data Fishery Resource Management Interdisciplinary Program, Chonnam National University, Yeosu, South Korea.
E-mail address: hysoh@jnu.ac.kr (H.Y. Soh).

https://doi.org/10.1016/j.ecolind.2023.110847
Received 19 June 2023; Received in revised form 8 August 2023; Accepted 18 August 2023
Available online 22 August 2023

Chu, 2008). Additionally, the East Asian monsoon occurs in summer, concentrating up to two-thirds of the annual rainfall in East Asia and over 40% of the summer rainfall during the rainy season (Kim et al., 2022). The pelagic ecosystem of the nECS is significantly influenced by the massive freshwater discharge from the Changjiang (Yangtze) River, in combination with the impact of the East Asian monsoon (Chen et al., 2008). The nECS has long been known as a highly productive fishing ground and has historically supported fishing activities and, more recently, the aquaculture industry (Zhang et al., 2019). The complexity of the water masses allows the nECS to maintain the characteristics of nutrient inflow and phytoplankton growth, which in turn preserves high zooplankton and fish productivity in marine ecosystems (Chen et al., 2017; Lee et al., 2019; Park et al., 2022).

The Intergovernmental Panel on Climate Change (IPCC) reported that global warming can increase the frequency and intensity of rainfall (Kimoto et al., 2005; Meehl et al., 2007; Jiang et al., 2008). In turn, large-scale rainfall events combined with anthropogenic activities such as dam construction can have a broader impact on marine ecosystems (Jiang et al., 2014; Liu et al., 2018; da Conceição et al., 2021). Since the establishment of the Three Gorges Dam, the nECS has undergone rapid environmental changes through artificial regulation of freshwater inflow (Wu et al., 2003; Wang, 2006). Many studies on zooplankton assemblages have primarily focused on the variation of assemblages due to rapid salinity changes, zooplankton distribution in the Changjiang River estuary region, medium- to long-term environmental changes and zooplankton assemblage structure, and indicator species of zooplankton (Chen et al., 2011; Gao et al., 2011; Wang et al., 2016; Wang et al., 2018; Lee et al., 2019; Shin et al., 2022). Furthermore, the analysis of marine environments has largely relied on vertical sampling methods, assuming that zooplankton is randomly distributed throughout the water column. However, because zooplankton communities often exhibit patchy and uneven distributions, vertical sampling alone cannot accurately reflect the distribution of zooplankton in different water masses (Folt and Burn, 1999). To address this limitation, various sampling devices such as MOCNESS (Multi Opening/Closing Net and Environmental Sampling System), which allows for continuous sampling at different depth layers, have been developed and adopted over the past decades (Wiebe et al., 1985).

In the nECS, the summer of 2020 was recorded as a period of continuous rainfall events that lasted for 60 days, thus ranking as the second-highest rainfall event by volume in the Changjiang River downstream since 1961 (Cui et al., 2021). To investigate the relationship between the vertically stratified distribution of zooplankton and the environmental factors influenced by the large influx of CDW in the nECS during summer, the study site was divided into three layers based on their hydrological uniformity: (1) surface mixed layer, (2) pycnocline layer, and (3) lower layer. The results were analyzed and compared with those of previous studies that employed continuous vertical sampling to examine the effects of water mass on zooplankton distribution in the nECS.

2. Materials and methods

2.1. Study area and sampling

The survey was conducted in the nECS from August 12 to 15, 2020, on board the Saedongbaek, the training ship of Chonnam National University, South Korea. The stations covered a latitude range of 32° to 33°N and a longitude range of 124° to 127.5°E, with a 0.5° interval spacing (Fig. 1). To obtain the sea water temperature, salinity, and fluorescence vertical profiles, conductivity-temperature-depth (CTD) and fluorescence (SBE 19 Plus, Sea-bird Electronics Inc., USA) meters were attached to the rosette sampler assemblage and cast from the surface to the bottom (5 m above the sea bed). For measuring suspended particulate matter (SPM) concentration, seawater was collected from the surface mixed layer (SML; 2–5 m), the chlorophyll-*a* maximum layer (CML), and the bottom layer using Niskin bottles attached to a rosette sampler assemblage. The collected 1 l seawater sample obtained from each layer was filtered using a pre-dried GF/F filter (pore size: 0.7 μm; 47 mm, GF/F, Whatman, Birmingham, UK). The filter papers were stored in a − 80 °C deep freezer before drying at 60 °C for 24 h in the laboratory. The weight of the filter papers was measured to a precision of 0.05 g and converted to mg L^{-1} (Korea's Ministry of Environment, 2020). The density of phytoplankton and protozoa was determined

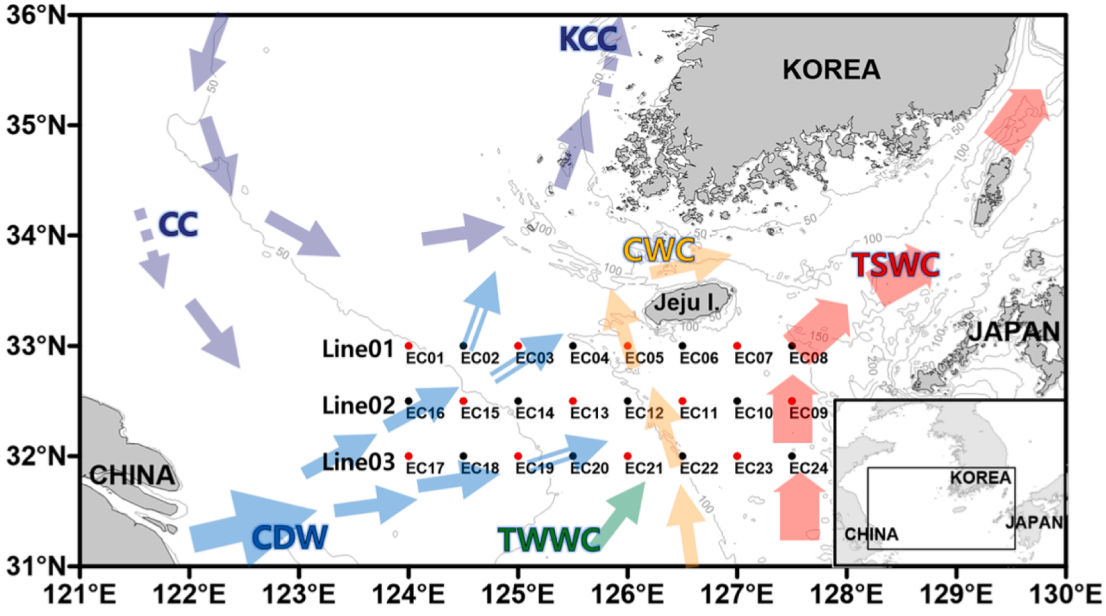

Fig. 1. Map of the sampling stations in the northern East China Sea in August 2020. The contour lines indicate the water depth (m). The circles indicate where the survey was performed, whereas the red circles indicate where the zooplankton samples were collected using MOCNESS. The arrows indicate the approximate positions of the main surface currents (modified from Lie and Cho, 2016; Cho et al., 2009): TSWC, Tsushima Warm Current; TWWC, Taiwan Warm Current; CDW, Changjiang diluted water; CC, China coastal current; CWC, Cheju Warm current; KCC, Korea coastal current.

using 1 l samples obtained from the SML and CML. The sample was fixed on board the research vessel using Lugol's solution to a final concentration of 2%. The fixed sample was concentrated 100 times to a final volume of 10 mL by repeatedly removing the supernatant after allowing the samples to sit undisturbed for more than 48 h in a plastic mass cylinder. After counting the phytoplankton and protozoan cells in 0.1 mL of the concentrated sample, the density of phytoplankton and protozoa was converted to cells mL^{-1}.

2.2. Zooplankton collection strategy and identification

Based on the CTD profiles, we divided the water strata into three distinct layers: (1) the surface mixed layer (SML), (2) the pycnocline layer (PNC), and (3) the lower layer (LL) (Table 1, Fig. 2). The zooplankton samples were collected from each layer at 12 stations with odd numbers by towing obliquely with a MOCNESS equipped with a net with a 1 m^2 mouth area and 200 μm mesh size (Figs. 1 and 2; Wiebe et al., 1985). The zooplankton samples were obtained using the same method regardless of the time of day (daytime and nighttime) from 10 m above the sea bed to the surface layer while ensuring stable operation and equipment safety. Zooplankton collection was scheduled for EC05; however, it could not be conducted due to a defect in the MOCNESS equipment.

The collected zooplankton was immediately fixed with neutralized seawater-formalin to a final concentration of 5% in the field. The amount of filtered seawater was calculated using a Tsurumi-Sikie-Kosakusho (TSK) flow meter (BESS Co. Ltd., USA) attached to the MOCNESS frame. In the laboratory, the samples were divided from 1/32 to 1/512 using a Motoda-type splitter. The zooplankton samples were then identified and counted on a UNESCO counting plate using a stereo microscope (SMZ 1000, Nikon, Japan). The classification system followed the guidelines of the WoRMS Editorial Board (2023).

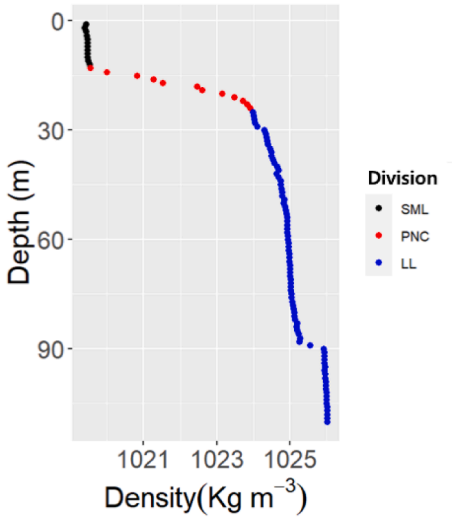

Fig. 2. Density profile at station EC23 for zooplankton sampling and division of water column. Abbreviations: SML, surface mixed layer; PNC, pycnocline layer; LL, lower layer.

Table 1
Information on the stations sampled with the MOCNESS sampler.

Station	Sampling date (2020)	Local time		Latitude (N°)	Longitude (E°)	Bottom depth (m)	Net opening depth (m)	Net closing depth (m)
		Start	End					
EC01	13 Aug.	3:42	3:54	32° 0.02′	124° 0′	43	36	15
							15	10
							10	0
EC03	15 Aug.	10:01	10:13	33° 0′	125° 0′	77	67	34
							34	14
							14	0
EC05	15 Aug.	16:45	16:56	32° 0.02′	126° 0′	100	78	29
							29	19
							19	0
EC07	15 Aug.	22:23	22:33	33° 0′	126° 0.02′	102	92	18
							18	14
							14	0
EC09	14 Aug.	9:40	9:55	32° 0.01′	127° 0.01′	128	118	20
							20	8
							8	0
EC11	14 Aug.	17:35	17:49	32° 0.01′	126° 0.01′	101	91	24
							24	14
							14	0
EC13	14 Aug.	22:57	23:10	32° 0.01′	125° 0.01′	68	58	32
							32	13
							13	0
EC15	15 Aug.	4:39	4:51	32° 0.01′	124° 0.01′	45	32	17
							17	8
							8	0
EC17	13 Aug.	10:41	10:54	31° 0.02′	124° 0′	36	26	15
							15	11
							11	0
EC19	13 Aug.	15:59	16:06	32° 0′	124° 0.02′	43	33	15
							15	8
							8	0
EC21	13 Aug.	21:34	22:02	32° 0′	126° 0′	77	67	32
							32	5
							5	0
EC23	14 Aug.	3:44	4:11	32° 0′	127° 0′	113	103	24
							24	12
							12	0

2.3. Visualization methods

The sea water temperature (°C), salinity, density (kg m^{-3}), and chlorophyll-*a* (Chl-*a*) concentration (μg L^{-1}) were averaged over every 1 m interval and classified according to the water depth of the SML, PNC, and LL. The average values were recalculated based on the aforementioned water depth divisions to visualize the horizontal distribution of different environmental factors. The horizontal distribution of the SPM concentration varied depending on each of the defined layers (SML, CML, and LL). The phytoplankton density was classified into diatoms, phytoflagellates, and dinoflagellates from each layer (SML and PNC, especially the subsurface chlorophyll maximum layer). As a potential food resource, protozoan density was included in the phytoplankton density plot. Abiotic and biotic factors, excluding zooplankton data, were visualized using the SURFER program (version 11, Golden Software Inc., USA). The zooplankton abundance and composition were divided into different water depth layers (SML, PNC, and LL) and visualized using the 'ggplot2' package in the R programming language (version 4.1.2).

2.4. Zooplankton assemblage analysis

To gain insights into the structure of the zooplankton communities in the study area, we conducted cluster analysis and non-metric multidimensional scaling ordination (nMDS). For the zooplankton assemblage analysis, we calculated the similarity distance for each layer using the Bray-Curtis dissimilarity distance based on the $\log_{10}(x+1)$-transformed zooplankton abundance. Next, we plotted the calculated similarity distance on a dendrogram using the Ward link method (Legendre and Legendre, 1998). To identify the optimal number of clusters, we used k-means, and the dendrograms for each layer were visualized with nMDS. Next, analysis of similarity (ANOSIM) was conducted to confirm the statistical significance of the identified groups in each layer. To compare the differences in zooplankton abundance among assemblage groups, we performed two-way ANOVA followed by Tukey's HSD (honestly significant difference) *post hoc* test. All statistical analyses were conducted in R (version 4.1.2).

2.5. Indicator species analysis

To identify zooplankton taxa that responded to changes in the marine environment, indicator values were calculated using the formula below (Dufrene and Legendre, 1997). The resulting IndVal index combines group specificity (A_{ij}) and group fidelity (B_{ij}) (Shi et al. 2018).

$$A_{ij} = \frac{\mathrm{Nind}_{ij}}{\mathrm{Nind}_{i.}}$$

$$B_{ij} = \frac{\mathrm{Nstn}_{ij}}{\mathrm{Nstn}_{.j}}$$

$$\mathrm{IndVal}_{ij} = A_{ij} \times B_{ij} \times 100$$

The variable i represents the species in the assemblage group, whereas j represents the stations included in the group. Nind_{ij} is the average abundance of species i in group j, and $\mathrm{Nind}_{i.}$ is the sum of the average abundance of species i in each group. Nstn_{ij} is the number of stations in group j where species i appeared, and $\mathrm{Nstn}_{.j}$ is the number of stations included in group j. An individual value of more than 50% ($p < 0.05$), higher than the previously reported 25% ($p < 0.05$), was used for our analysis (Dufrene and Legendre, 1997). The indicator value of zooplankton species was calculated using the IndVal function of the 'indicspecies' package (Caceres and Legendre, 2009).

2.6. Correlation analysis between environmental variables and zooplankton abundance

To analyze the correlation between environmental variables and zooplankton abundance, we first normalized the environmental

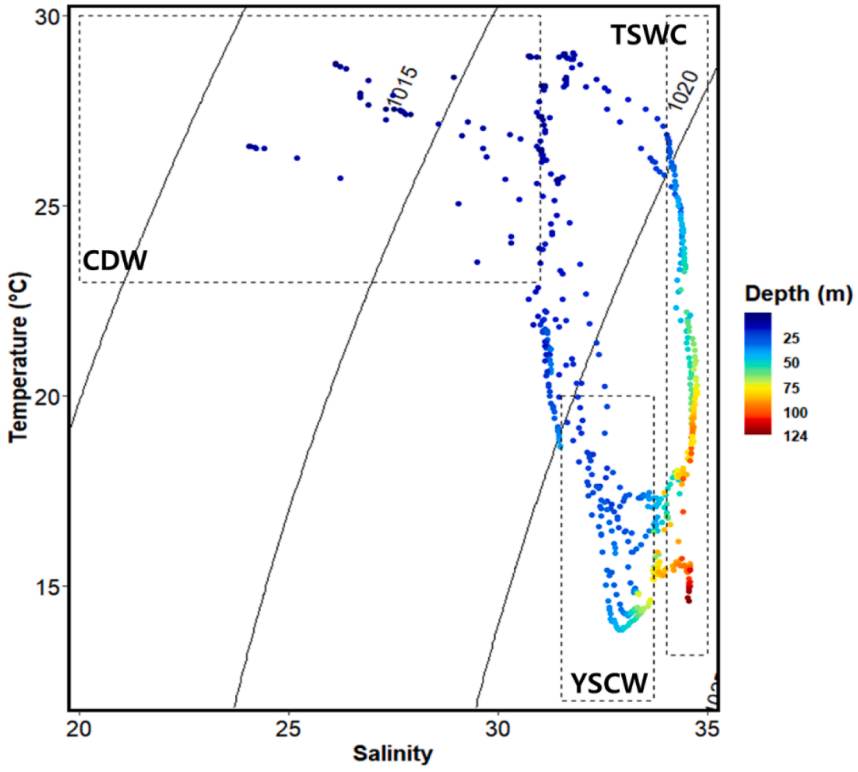

Fig. 3. T-S diagram of water column at sampling stations. The colors indicate seawater depth. Abbreviations: YSCW, the Yellow Sea Cold Water by Hur et al. (1999); CDW, the Changjiang Diluted Water by Lie et al. (1984); TSWW, the Tsushima Warm Water by Kim et al. (2020).

variables of each layer to the Z-score and $\log_{10}(x + 1)$-transformed the indicator species abundance. Next, we performed canonical correspondence analysis (CCA) and calculated the Spearman correlation coefficient ($p < 0.05$). Correlation analysis (CA) was conducted using R (version 4.1.2).

3. Results

3.1. Environmental variables

During the study period, the seawater temperature ranged from 13.8 to 29.9 °C (Fig. 3a). The eastern part of the sampling area exhibited higher seawater temperatures across the entire water column, with particularly elevated temperatures observed in the northeastern region, including the PNC and LL (Fig. 4a-c). In the SML, the seawater temperature ranged from 25.6 to 29.9 °C. The seawater temperature in the SML displayed a small horizontal difference and remained, on average, higher than that of PNC and LL (Fig. 4a) (ANOVA, $p < 0.001$). In the PNC, the seawater temperature ranged from 14.5 to 29.0 °C. The seawater temperature in the central region of the PNC was approximately 5 °C lower than that of its surrounding areas (Fig. 4b). The area with lower seawater temperature was observed across the LL, with temperatures ranging from 13.8 to 16.2 °C (Fig. 4c). Higher seawater temperatures were more densely distributed in the open sea area than in the shallow coastal area for both PNC and LL (Fig. 4b and 4c). The salinity ranged from 24.0 to 31.8 in the SML, from 26.2 to 33.9 in PNC, and from 31.0 to 34.7 in the LL (Fig. 3a). Salinity tended to increase throughout the water column with increased distance from the Chinese coast. The difference in salinity was clear in the SML, but this difference decreased with depth (Fig. 4d-f). Density ranged between 1,014.8 and 1,025.1 kg m^{-3} (Fig. 4g-i). The SML exhibited a similar pattern to that of the salinity data, whereas the patterns of the PNC and LL were more consistent with those of the temperature data (Fig. 4g-i).

The SPM concentration ranged from 6.5 to 21.5 mg L^{-1} (Fig. 5d-f). Particularly, station EC09 exhibited the highest concentration of 21.7 mg L^{-1} at the LL (Fig. 5f). However, no consistent trend was observed in the SML and the PNC. The Chl-*a* concentration ranged from 0.1 to 2.9 μg L^{-1} (Fig. 5a-c). Moreover, while the concentration decreased gradually in the SML as the sampling stations were farther away from China, no consistent trend was observed in the PNC and LL (Fig. 5b and 5c). The density of the phytoplankton and the protozoan in the SML ranged from 1.1×10^3 to 871.8×10^3 cells mL^{-1}, with dinoflagellates being identified as the dominant group, peaking at 21.1%–98.25%. In the CML layer, the density of the phytoplankton and the protozoan also ranged from 1.1×10^3 to 871.8×10^3 cells mL^{-1}. Diatoms were predominant in EC17 and EC19 with a percentage range of 7.9%–96.5% in the CML. In contrast, protozoan and phytoflagellates were the dominant groups in the CML of the central and eastern parts of the survey area, with percentage ranges of 0.3%–64.2% and 1.6%–37.8%, respectively (Fig. 5).

3.2. Zooplankton distribution

The zooplankton abundance in the SML ranged from 104 to 16,073 ind. m^{-3} (mean: 4,980 ind. m^{-3}) (Fig. 6a) and tended to increase from west to east in Line03, whereas it exhibited a decreasing trend in the same direction in Line02 (Fig. 6a). In the PNC, the zooplankton abundance ranged from 172 to 15,401 ind. m^{-3} (mean: 4,744 ind. m^{-3}) (Fig. 6b). The highest abundance was observed at a depth of 100 m in the central part of both lines in the PNC. The lowest mean zooplankton abundance was observed in the LL, ranging from 384 to 6,558 ind. m^{-3} (mean: 2,682 ind. m^{-3}) (Fig. 6c). There were no significant differences in the zooplankton abundances between the water layers (p greater than 0.05). A total of 99 taxa were identified in 11 of the examined stations with three water layers (Fig. S1). A total of 9 taxonomic groups were found to be dominant based on their relative abundance (Fig. 7). In the SML, the dominant groups were copepods (44.4%–88.3%), meroplankton (0.2%–18.8%), and thaliaceans (1.4%–15.7%) (Fig. 7). In the PNC, the dominant groups were copepods (44.2%–98.0%), chaetognaths (0.6%–31.7%), and meroplankton (0.2%–28.9%) (Fig. 7). In the LL, the dominant groups were copepods (1.2%–91.2%), meroplankton (0.3%–69.0%), and malacostracans (0.3%–20.2%) (Fig. 7).

The relative abundance of copepods increased from west to east in the survey area, whereas it decreased from the SML to the LL (Fig. 7). Branchiopods and ostracods were mainly found in the eastern part of the survey area. The relative abundance of brachiopods decreased vertically from the SML to LL, whereas the relative abundance of ostracods tended to increase (Fig. 7). Hydrozoans were also found in the eastern part of the surveyed area. The relative abundance of hydrozoans was higher in the SML at station EC07 and in the LL at station EC09 (Fig. 7). Thaliaceans were mainly distributed in the western part of Line02 and Line03 in both the SML and the PNC. Malacostracans were distributed in the LL of all stations (Fig. 7). Meroplankton exhibited a high proportion in the

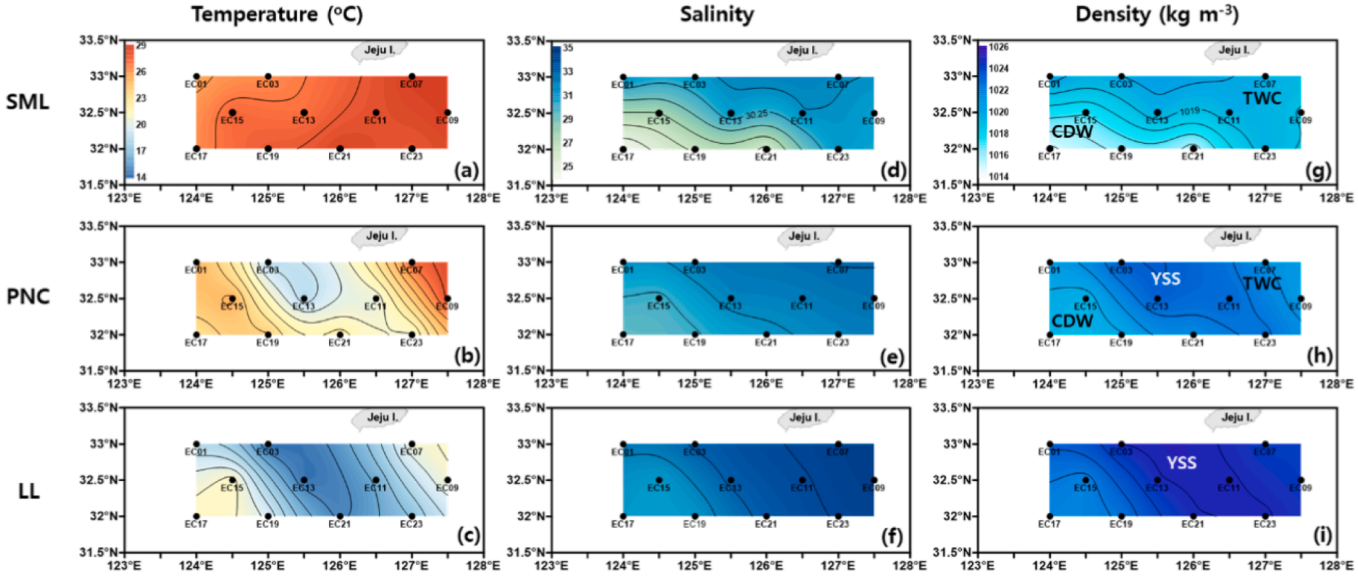

Fig. 4. Horizontal distribution of (a-c) mean temperature, (d-f) mean salinity, and (g-i) mean density with the water mass distribution in reference in (a, d, g) the SML, (b, e, h) PNC, and (c, f, i) LL.

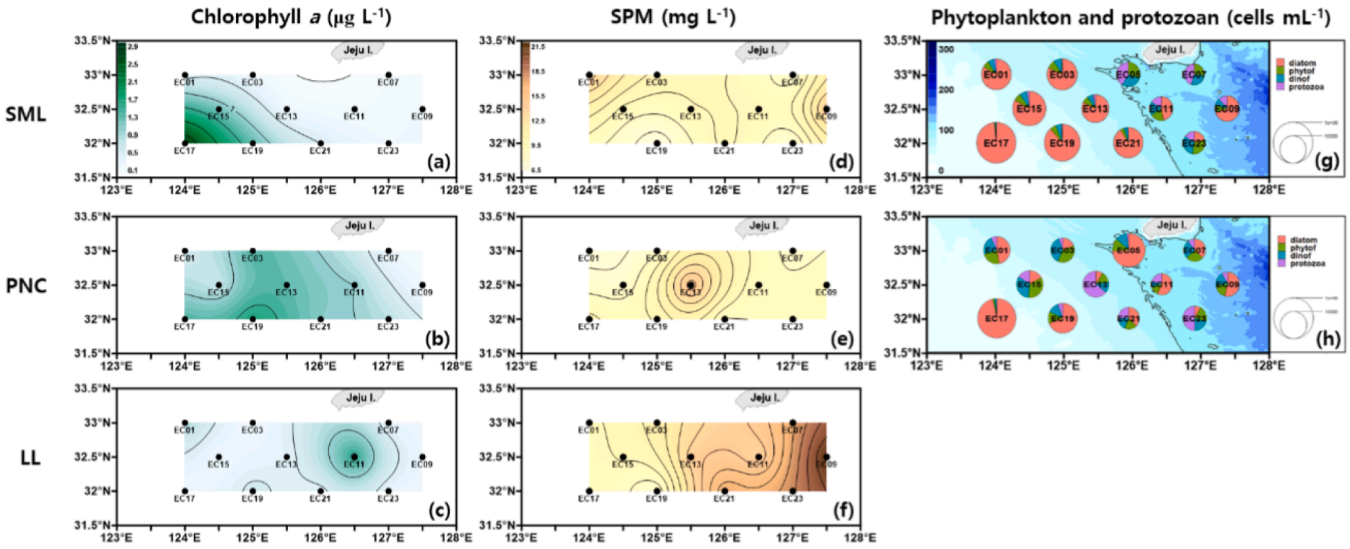

Fig. 5. Same as Fig. 4, but (a-c) mean Chl-*a*, (d-f) SPM on each layer, and (g, h) density of phytoplankton and protozoan on each layer.

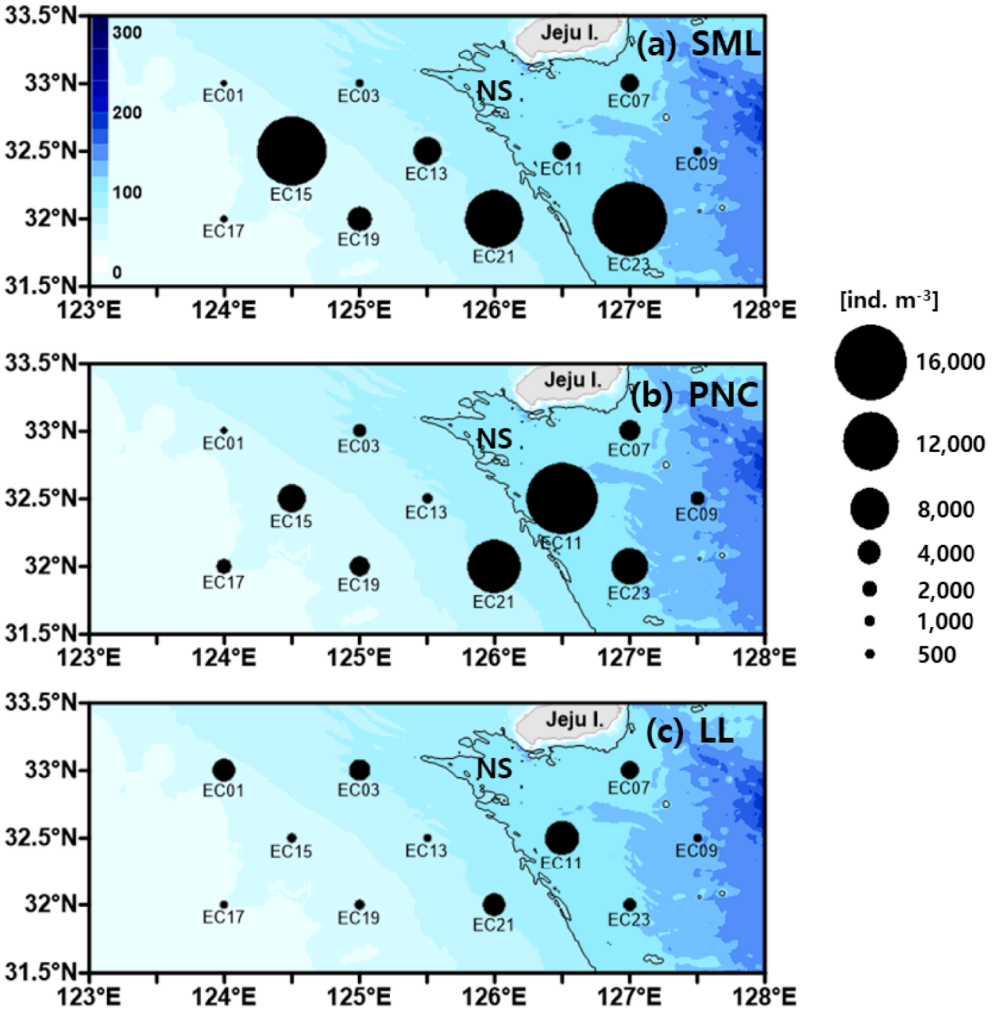

Fig. 6. Horizontal distribution of zooplankton abundance in (a) the SML, (b) PNC, and (c) LL. Abbreviations: NS, not sampled.

northwestern part of the surveyed area and was relatively more abundant in the LL (Fig. 7), with the highest dominance of meroplankton being observed at station EC19 in the LL (Fig. 7).

3.3. Zooplankton assemblage and structure

Hierarchical clustering classification and nMDS were performed based on the abundance of zooplankton identified at the species level

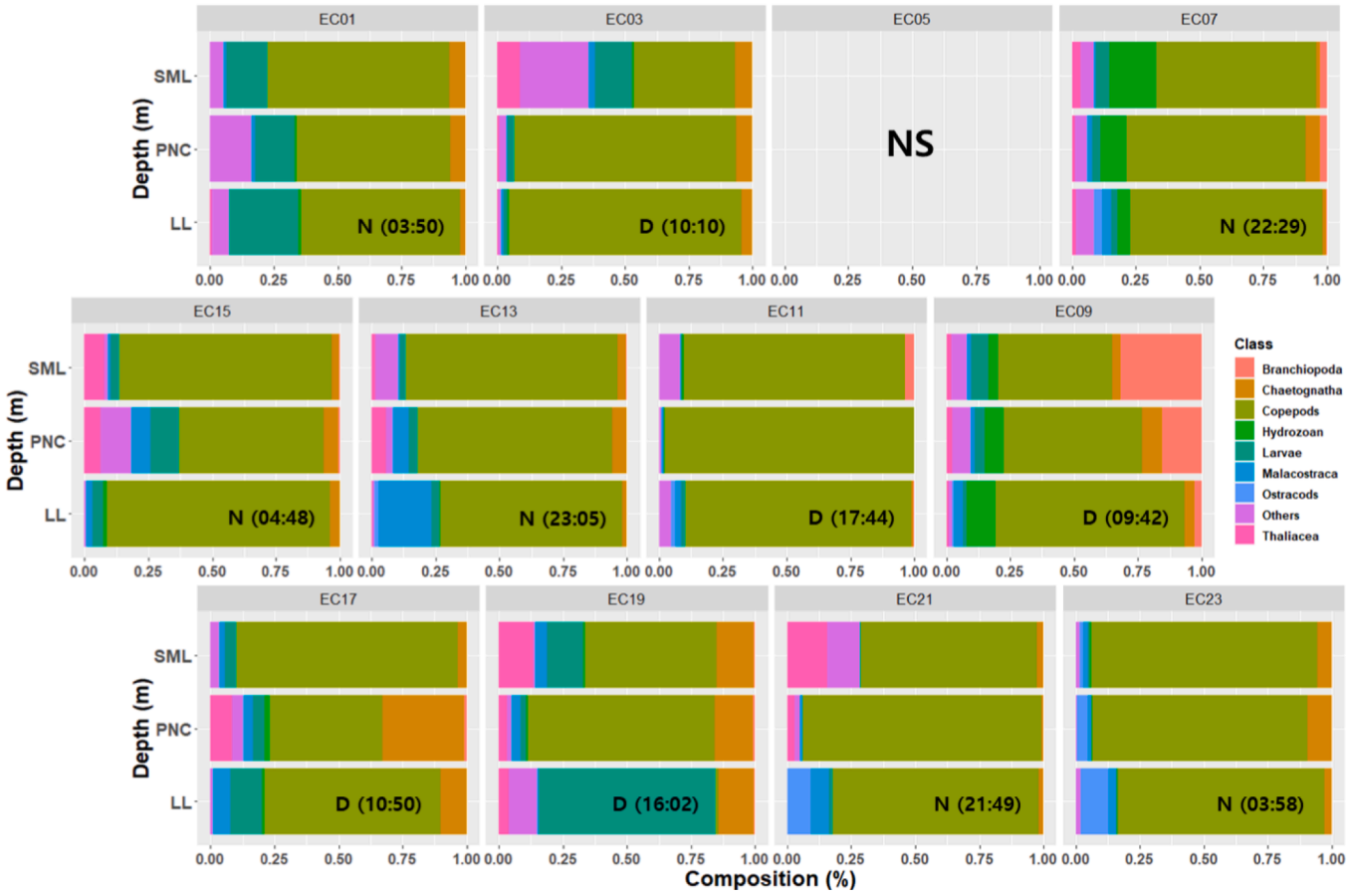

Fig. 7. Relative abundance of zooplankton at each station and layer with 9 taxonomic groups. Abbreviations: NS, not sampled.

(Fig. 8). In the SML, the zooplankton assemblage was divided into three groups with an nMDS stress value of 0.05 ($p < 0.01$) (Table 2, Fig. 8a). The abundance of zooplankton in group SA ranged from 43 to 65 ind. m^{-3} (mean: 54 ind. m^{-3}) (Fig. 9a). The dominant taxa in group SA were *Paracalanus parvus* s. l. (21.2%–54.6%), *Calanus sinicus* (2.3%–39.4%), and *Ditrichocorycaeus affinis* (2.3%–9.1%) (Fig. 9d). The abundance of zooplankton in group SB ranged from 262 to 6,881 ind. m^{-3} (mean: 3,488 ind. m^{-3}) (Fig. 9a). The dominant species in group SB were *P. parvus* s. l. (0.8%–95.0%) and *Acartia pacifica* (0.6%–81.2%) (Fig. 9d). Group SC consisted of three stations located northeast of the survey area. The abundance of zooplankton in group SC ranged from 292 to 1,043 ind. m^{-3} (mean: 702 ind. m^{-3}) (Fig. 9a). The dominant species in group SC were *Oncaea* spp. (12.7%–62.0%), *P. parvus* s. l. (1.7%–59.2%), Others (7.6%–27.5%), and *Pseudevadne tergestina* (5.4%–53.3%) (Fig. 9d). Pairwise tests revealed that Group SA differed from both group SB and SC ($p < 0.05$) (Table 2).

In the PNC, the zooplankton assemblage was divided into three groups with an nMDS stress value of 0.046 ($p < 0.01$) (Table 2, Fig. 8b). Group PA included six central stations crossing the survey. The abundance of zooplankton in group PA ranged from 62 to 4,730 ind. m^{-3} (mean: 1,808 ind. m^{-3}) (Fig. 9b). The dominant taxa in group PA were *Paracalanus parvus* s. l. (38.3%–84.2%) and *Calanus sinicus* (2.7%–44.7%) (Fig. 9e). Group PB included two southwest stations. The abundance of zooplankton in group PB ranged from 149 to 1,456 ind. m^{-3} (mean: 803 ind. m^{-3}) (Fig. 9b). The dominant species in group PB were *Acartia pacifica* (63.9%–94.2%) and *P. parvus* s. l. (0.3%–13.9%) (Fig. 9e). Group PC included three stations located in the eastern region of the survey area. The abundance of zooplankton in group PC ranged from 752 to 2,331 ind. m^{-3} (mean: 1,537 ind. m^{-3}) (Fig. 9b). The dominant species in group PC were *P. parvus* s. l. (2.2%–57.0%), *Oncaea* spp. (30.9%–72.4%), Others (14.3%–28.2%), and *Pseudevadne tergestina* (4.8%–32.5%) (Fig. 9e). Pairwise tests showed that Group PA differed from the remaining groups ($p < 0.05$) (Table 2).

In the LL, the zooplankton assemblage was divided into two groups with an nMDS stress value of 0.042 ($p < 0.01$) (Table 2, Fig. 8c). Group LA included seven central stations from the west to the middle of the survey area. The abundance of zooplankton in the LA group ranged from 123 to 1,553 ind. m^{-3} (mean: 839 ind. m^{-3}) (Fig. 9c). The dominant taxa in group LA were *Calanus sinicus* (2.9%–95.6%) and *Paracalanus parvus* s. l. (12.6%–76.0%) (Fig. 9f). Group LC included four stations from the middle to the east. The abundance of zooplankton in group LC ranged from 10 to 2,030 ind. m^{-3} (mean: 965 ind. m^{-3}) (Fig. 9c). The dominant taxa in group LC were *Oncaea* spp. (30.1%–60.0%), Others (25.6%–50.0%), and *P. parvus* s. l. (2.0%–32.7%) (Fig. 9f). Moreover, pairwise tests revealed that there was a statistically significant difference between Group LA and Group LC ($p < 0.05$) (Table 2).

3.4. Associations between zooplankton species and environmental factors

IndVal analysis was conducted based on the identified groups of zooplankton to assess the indicator species using the zooplankton abundance (Table 3). Species with an indicator index greater than 50 and with statistical significance were selected as indicator species (Table 3). In the SML, *Acartia pacifica* and *Calanus sinicus* were selected as indicators for group SB, whereas *Ctenocalanus vanus* and *Labidocera acuta* were selected as indicators for group SC (Table 3). In the PNC, *Calanus sinicus* and *Paracalanus parvus* s. l. were selected as indicators for group PA, and *Undinula vulgaris*, *Pleuromamma gracilis*, *Calocalanus* sp., and *Temora discaudata* were selected as indicators for group PC (Table 3). In the LL, *Calanus sinicus* was selected as an indicator for group

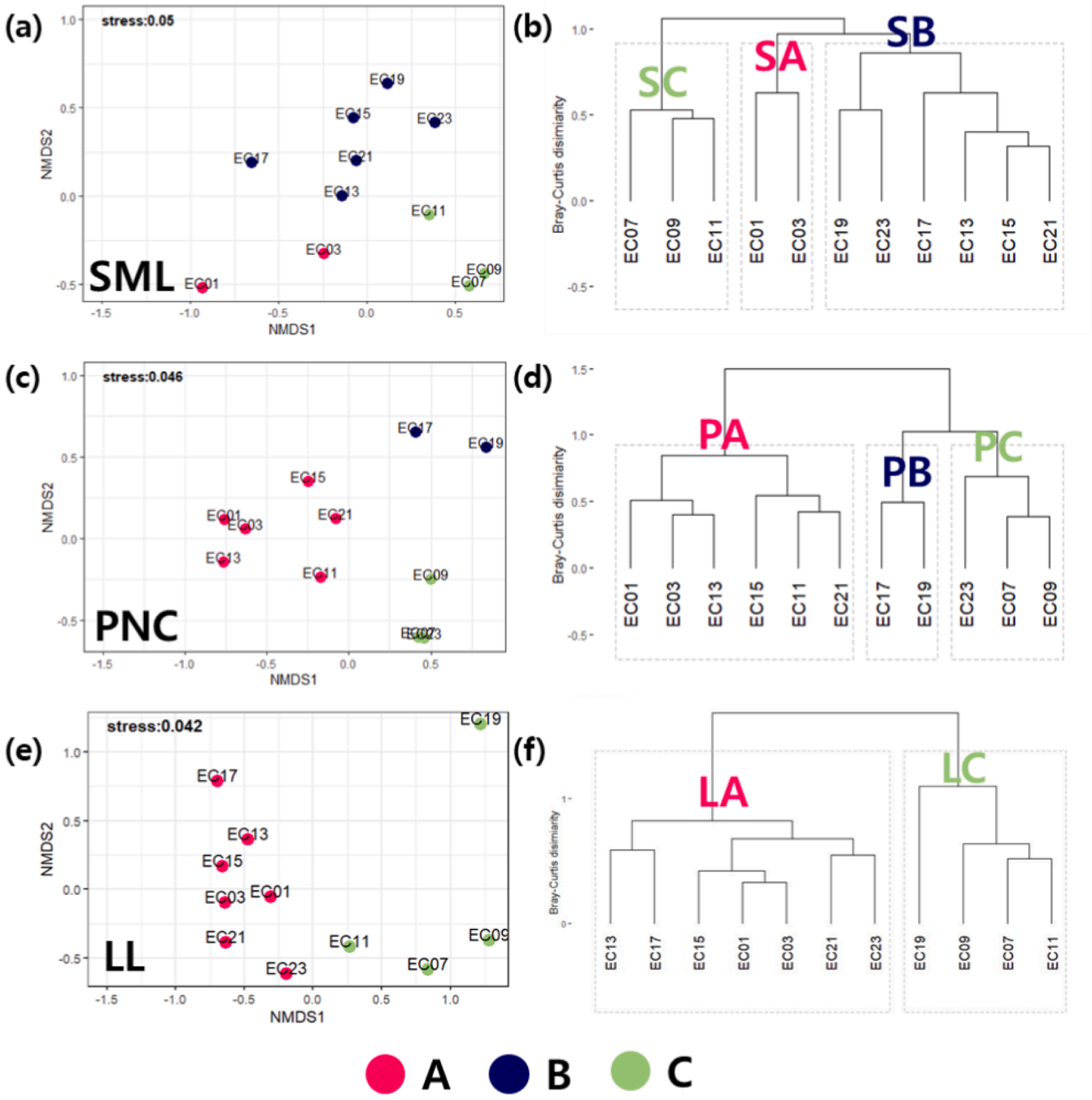

Fig. 8. Nmds (a, c, e) and dendrogram (b, d, f) of stations similarity based on cluster analysis of zooplankton abundance in (a, b) the sml, (c, d) pnc, and (e, f) ll.

LA, whereas *Ctenocalanus vanus, Clausocalanus farrani*, *Clausocalanus arcuicornis, Clausocalanus minor*, and *Pseudevadne tergestina* were selected as indicators for group LC (Table 3).

In the CCA results of the SML, the first axis explained 76.1% of the data distribution, whereas the second axis explained 23.4% of the data distribution (Table 4). The Chl-*a* concentration and the density of diatoms, phytoflagellates, and protozoans showed a positive correlation with axis 1, whereas seawater density, salinity, and SPM concentration showed a positive correlation with axis 2 (Fig. 10a). *Ctenocalanus vanus* (CV) and *Labidocera acuta* (LA) showed a positive correlation with water temperature, salinity, and density but a negative correlation with Chl-*a* concentration, as well as the density of diatoms, phytoflagellates, dinoflagellates, and protozoans (Fig. 10b). *Calanus sinicus* (CS) exhibited a negative correlation with temperature, whereas *Acartia pacifica* (AP) showed a positive correlation with Chl-*a* concentration and the density of phytoflagellates, diatoms, and a negative correlation with salinity and seawater density (Fig. 10b). According to the CCA results of the PNC, the first axis explained 87.1% of the data distribution and the second axis explained 7.9% (Table 4). The water temperature and salinity had a positive correlation with axis 1, whereas Chl-*a* concentration and the density of diatoms, dinoflagellates, and phytoflagellates had a positive correlation with axis 2 (Fig. 10c). *Calanus sinicus* (CS) had a strong negative correlation with water temperature and a positive correlation with Chl-*a* concentration (Fig. 10d). *Paracalanus parvus* s. l. (PP s. l.) showed a negative correlation with water temperature and a weak positive correlation with density and Chl-*a* concentration (Fig. 10d).

Table 2
Results of ANOSIM analysis for zooplankton assemblage.

Global test		R	*p*
SML		0.779	0.002
PNC		0.904	0.001
LL		0.765	0.003
Pairwise tests*		R	*P*
SML	SA-SC	1	0.100
	SA-SB	0.891	0.048
	SC-SB	0.621	0.036
PNC	PA-PC	0.895	0.012
	PA-PB	0.885	0.036
	PC-PB	1	0.100
LL	LA-LC	0.765	0.003

*Note: The letters S, P, and L refer to the surface, pycnocline, and lower layer, respectively, whereas A, B, and C indicate the distinct clusters obtained from cluster analysis based on zooplankton abundance [refer to Fig. 8 (b, d, f) for more details on the clustering results].

Pleuromamma gracilis (PG), *Calocalanus* sp. (Calo sp.), *Temora discaudata* (TD), and *Undinula vulgaris* (UV) had a positive correlation with temperature and salinity but a negative correlation with Chl-*a* concentration and the density of phytoflagellates and dinoflagellates (Fig. 10d). For the CCA results of the LL, the first axis explained 92.0% of the data distribution, whereas the second axis explained 4.9% (Table 4). The water temperature, salinity, SPM concentration, density, and Chl-*a* concentration showed a positive correlation with axis 1 (Fig. 10e). *Calanus sinicus* (CS) had a negative correlation with salinity and SPM concentration, while *Clausocalanus arcuicornis* (ClA), *Cl. minor* (ClM), *Cl. farrani* (ClF), *Ct. vanus* (CV), and *Pseudevdne tergestina* (PsT) showed a positive correlation with salinity and SPM concentration (Fig. 10f).

4. Discussion

Our study revealed that the distribution of water masses had a significant impact on the composition and abundance of zooplankton communities in each layer. Instead of observing a single cluster in each specific sampling area, we identified multiple vertically distributed communities in the sampled stations (Figs. 9 and 11). Although confirming the continuity of the zooplankton assemblages in each layer was challenging, we found consistency among the groups in terms of water mass continuity, zooplankton species composition, and abundance (Figs. 3 and 9). The identified assemblages in each layer were marked as similar clusters. This approach effectively reflected the vertical stratification of the water column, allowing us to overcome the limitations of vertical collection and obtain more detailed information on the water mass structures through cluster analysis and vertical arrangement of the proposed assemblage groups. Unlike previous studies that relied on vertical sampling in the northern East China Sea, our approach provided novel insights into the vertical structure of water masses and their association with zooplankton communities.

The study area exhibited a salinity gradient from Line 03 to other

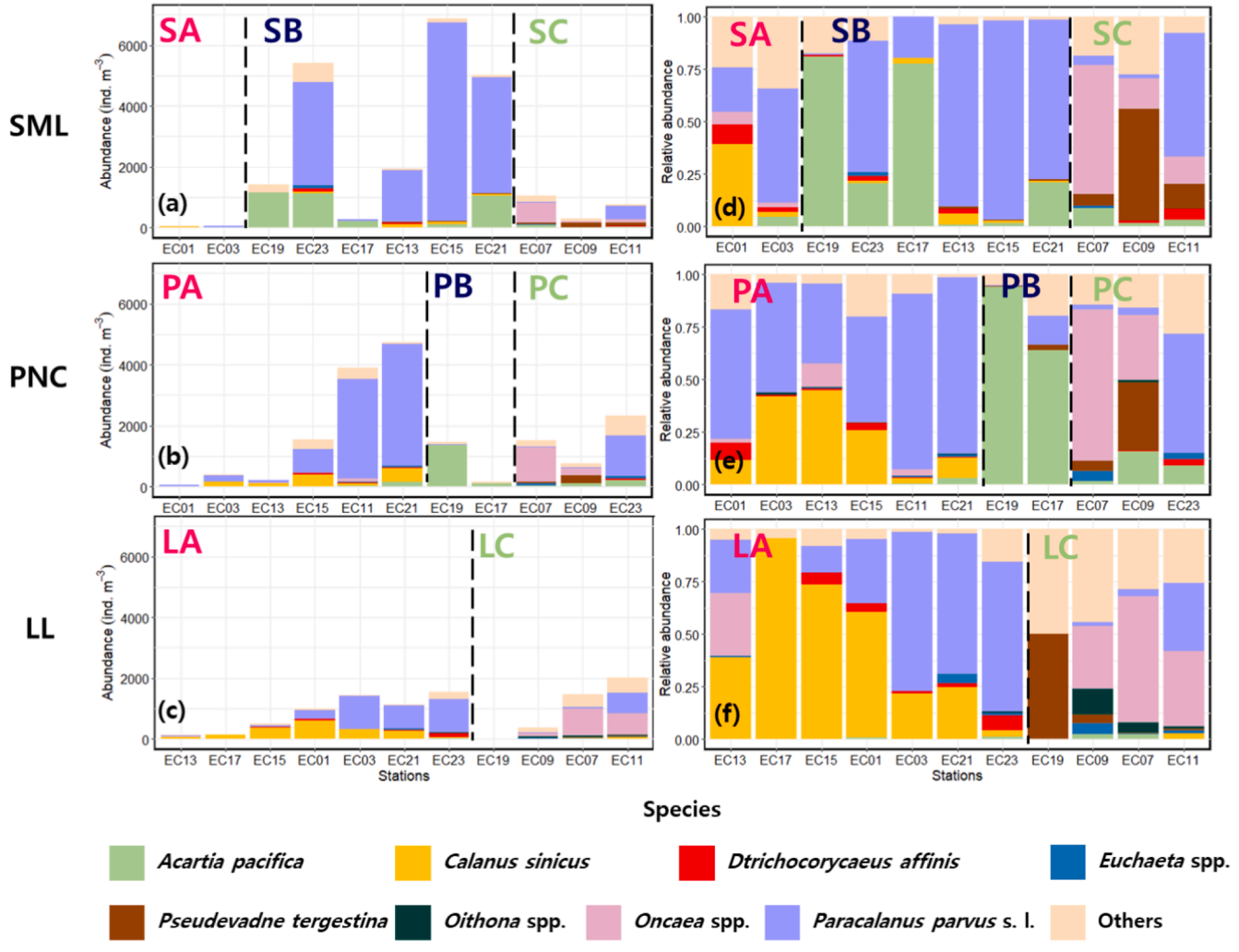

Fig. 9. Distribution of dominant taxa by assemblage group in (a, d) the SML, (b, e) PNC, and (c, f) LL.

Table 3
IndVal analysis of zooplankton assemblages determined by dendrogram plot considering each depth. The values were deemed indicative of major indicator species (Indicator index ≥ 50 and significantly statistical value $p < 0.05$).

Depth	Taxa	IndVal (%)	*p* value	Association
SML	***Acartia pacifica***	75	0.008	SB
	Calanus sinicus	69	0.042	SB
	Ctenocalanus vanus	100	0.004	SC
	Labidocera acuta	100	0.004	SC
PNC	***Calanus sinicus***	100	0.002	PA
	***Paracalanus parvus* s. l.**	71	0.042	PA
	Undinula vulgaris	100	0.005	PC
	Pleuromamma gracilis	100	0.005	PC
	***Calocalanus* sp.**	100	0.005	PC
	Temora discaudata	90	0.005	PC
LL	***Calanus sinicus***	95	0.008	LA
	Pseudevadne tergestina	86	0.003	LC
	Clausocalanus minor	86	0.021	LC
	Clausocalanus arcuicornis	86	0.021	LC
	Clausocalanus farrani	82	0.021	LC

lines, with the lowest salinity observed in Line 03, and a vertical salinity gradient from the SML to the PNC (Fig. 4d-f). This salinity variation was attributed to runoff from the Changjiang River and heavy precipitation entering the nECS during the summer (Chen et al., 1994). In 2020, there was a significant increase in precipitation in the Three Gorges Region (TGR) of the Changjiang River compared to the annual average and the previous year, leading to heightened freshwater input (Cui et al., 2021). Numerical models by Chang and Isobe (2003) indicated that the salinity of the CDW ranged from 26 to 32. Areas with lower salinity in the SML showed higher concentrations of chlorophyll-*a* (Chl-*a*), whereas Chl-*a* concentrations decreased with increasing salinity (Fig. 4d, 5a). The influx of the CDW into the nECS is consistent with previous studies showing an increase in Chl-*a* concentrations or phytoplankton density (Fig. 5g-h; Park et al., 2022). Notably, the stations directly influenced by the dilute waters of the Changjiang River showed the highest proportion of diatoms (46.88% to 91.20%) in the SML and PNC (Fig. 5g-h). These findings highlight the strong influence of the CDW on the surface layer of the study area.

In the northwest of the survey area, the observed cold water showed a difference of<2 °C from the surrounding area in the SML. However, the difference in water temperature increased to more than 5 °C from the PNC to the LL, dividing the center of the surveyed area (Fig. 4a-c). The presence of a cold water mass in the bottom layer of the Yellow Sea, gradually moving southward from spring to autumn, is widely known. Additionally, the cold water mass formed in the Yellow Sea during winter remains at the bottom of the thermocline layer (Nakao, 1977). While there is still insufficient statistical evidence to conclusively support the southward flow of cold water from the bottom of the Yellow

Table 4
Summary of canonical correspondence analysis (CCA) for the zooplankton matrix with environmental variables used as constraints.

CCA	SML		PNC		LL	
	CCA1	CCA2	CCA1	CCA2	CCA1	CCA2
Eigenvalue	0.5265	0.1621	0.6459	0.0586	0.8335	0.0822
Proportion (%)	76.1	23.4	87.1	7.9	85.9	8.5
Accumulative proportion (%)	76.1	99.5	87.1	95.0	85.9	94.4

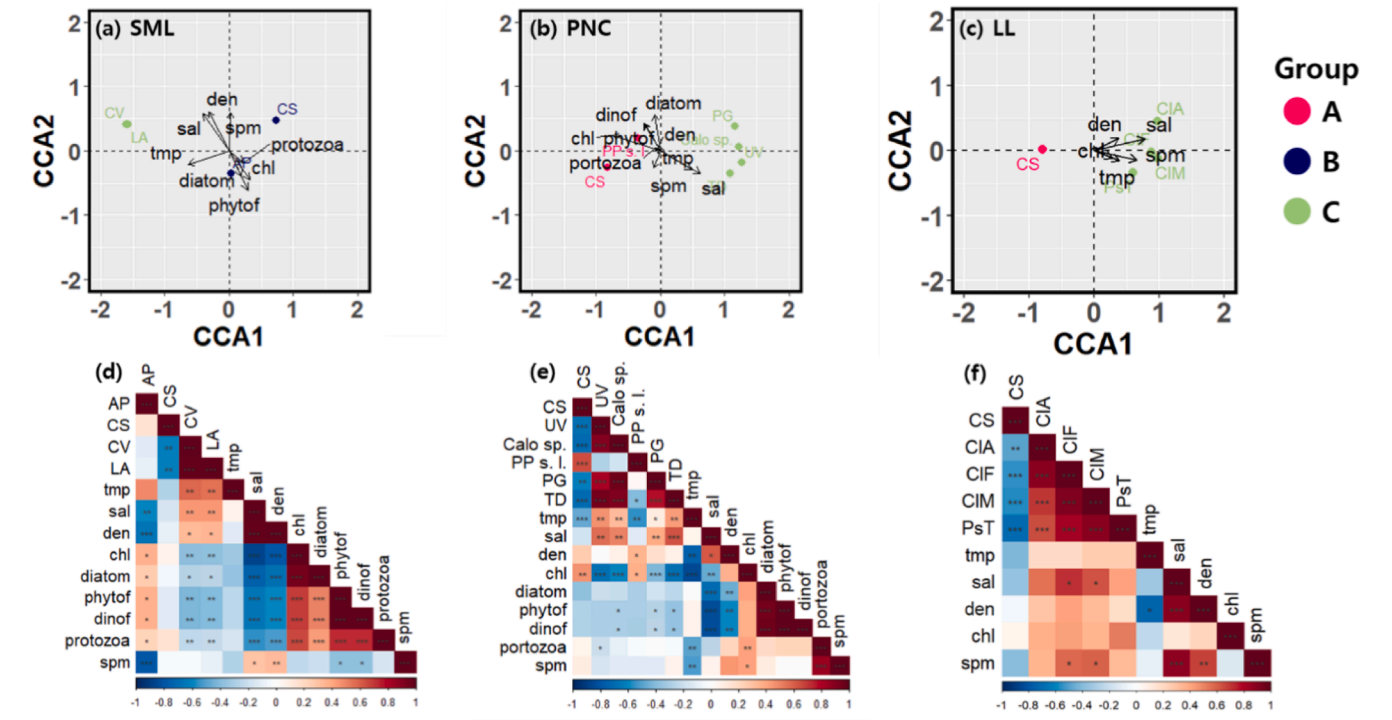

Fig. 10. Canonical correspondence analysis (CCA) ordination plot and correlation analysis (CA). (a, d) CCA plot and CA matrix for SML, (b, e) CCA plot and CA matrix for PNC, (c, f) CCA plot and CA matrix for LL. The asterisks indicate significant correlations (*: $p < 0.05$, **: $p < 0.01$, ***: $p < 0.001$). Abbreviations: CV, *Ctenocalanus vanus*; LA, *Labidocera acuta*; CS, *Calanus sinicus*; AP, *Acartia pacifica*; PP s. l., *Paracalanus parvus* s. l.; PG, *Pleuromamma gracilis*; Calo sp., *Calocalanus* sp.; TD, *Temora discaudata*; UV, *Undinula vulgaris*; ClA, *Clausocalanus arcuicornis*; ClM, *C. minor*; ClF, *C. farrani*; PsT, *Pseudevdne tergestina*; tmp, temperature; sal, salinity; den, density; chl, chlorophyll-*a*; phytof, phytoflagellate; dinof, dinoflagellate; spm, suspended particle matter.

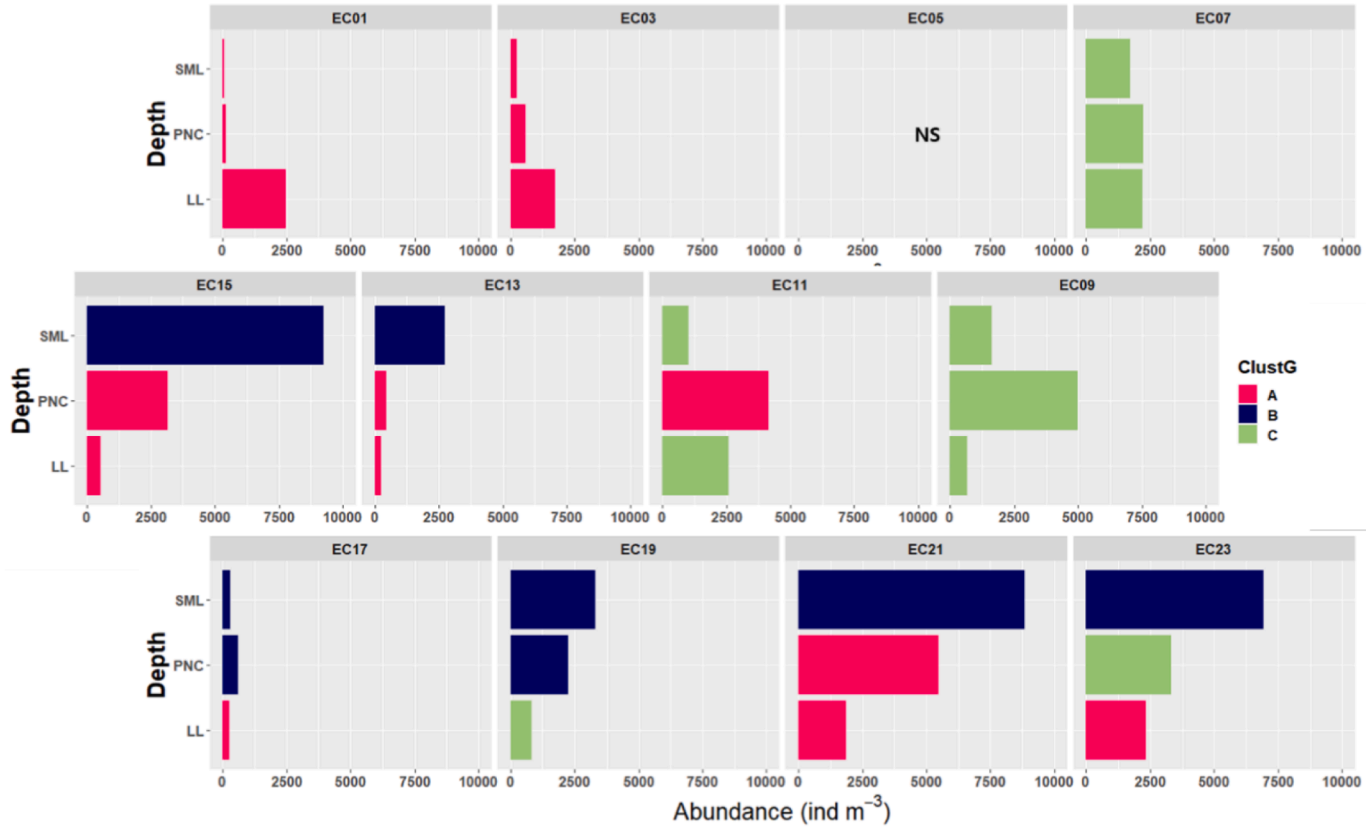

Fig. 11. Vertical distribution of zooplankton abundance used in cluster analysis in August 2020. Each color represents different groups based on zooplankton abundance in each layer. Abbreviations: NS, not sampled.

Sea, Jang et al. (2011) proposed that the mixed water observed in the southern Yellow Sea and the southeast sea of Jeju contains the cold water from the bottom of the Yellow Sea. Although directly characterizing the bottom cold water in the study area is challenging, this phenomenon may be attributed to the mixing of the cold water from the Yellow Sea and the continental shelf water during summer.

Relatively higher water temperatures were observed in the eastern SML of the study area. In the PNC, elevated values of average temperature above 27 °C and average salinity above 32.5 were observed at stations EC07 and EC09, and in the LL, high temperatures above 22 °C and average salinity above 34.4 were observed at stations EC07 and EC09, indicating the clear influence of TSWC in all layers (Figs. 3 and 4). The TSWC, a branch of the Kuroshio Current, is known to flow northward across the study area, transporting the Taiwan Warm Water (TWW), which is a mixture of Kuroshio Current water with continental shelf waters (Kondo, 1985; Seung, 1992).

Copepods were the most dominant or subdominant taxa in all layers of the survey area (Fig. 7). In the SML, group SA included two northwestern stations (EC01, 03) where water temperatures were about 2 °C lower than those in the surrounding waters (Fig. 4). Compared to groups SB and SC, species in group SA occupied a high relative abundance, such as *Calanus sinicus, Ditrichocorycaeus affinis, Acartia omorii,* and *Euphausia pacifica* (Fig. 9 and S1). However, no species with an indicator power exceeding 50% (also, 25%) were identified in group SA (Table 3). Due to the inclusion of only two stations in this group, it is presumed that statistically significant species were not extracted.

The distribution of group SB mainly includes six stations where the salinity concentration was low. However, the abundance pattern of Line03 and Line02 showed opposite trends (Fig. 6a). In Line02, the total zooplankton abundance decreased as the distance from the Changjiang River estuary increased, whereas in Line03, the total zooplankton abundance increased with the distance from the Changjiang River estuary (Fig. 6a). Notably, the relative abundance of *Acartia pacifica* was high on the lower salinity side, and as the salinity gradually increased, the abundance and relative abundance of *Paracalanus parvus* s. l. also increased. While *Acartia pacifica* and *P. parvus* s. l. are known to be dominant species in the coastal waters of China and the Yellow Sea during summer, our study confirms that their distribution extended to the open ocean area up to station EC23 (Fig. 9; Tseng et al., 2008; Hsiao et al., 2011). The occurrence of neritic species from the coast to the offshore area in the SML can be attributed to the transport of individuals facilitated by the expansion of the CDW (Grieco et al., 2005). Indicator species of group SB also showed a significantly positive correlation with salinity.

Group SC included three eastern stations (EC07, EC09, and EC11). The zooplankton species diversity of group SC was higher than that of groups SA and SB, and *Oncaea* spp. and *Pseudevadne tergestina* were present at a high relative abundance. In the SML, an additional 11 indicator species of warm currents, including *Nannocalanus minor*, appeared only in group SC (Fig. S1). Group SC was mainly distributed in the region with the highest average seawater temperature compared to the entire water column in the surveyed area (Fig. 4a). Moreover, the indicator species in group SC showed statistically significant positive correlations with seawater temperature and salinity, and negative correlations with Chl-*a*, phytoplankton, and protozoan (Fig. 10a and 10b).

In the PNC, group PA included six central stations located in areas where the water temperature distribution was approximately 5 °C lower than the temperature of adjacent stations (Fig. 4b). The total abundance trend was higher in the southeast stations (EC11 and EC21) where the influence of cold water was relatively weak compared to the northwest stations (EC01, EC03, EC13, and EC15) where the influence of cold water was strong. The relative abundance of *Calanus sinicus* was higher in the northwest stations, whereas *Paracalanus parvus* s. l. was dominant in the southeast stations (Fig. 9e). *Calanus sinicus* is widely distributed in

the Northwestern Pacific continental shelf and shows a preference for lower seawater temperatures (Wang et al., 2003). Additionally, the distribution of Malacostraca (*Euphausia pacifica*) was consistent with the distribution of cold water observed in group PA (Fig. 6). The observed temperature range and distribution of cold water in group PA could be related to the advection of cold water from the Yellow Sea. The indicator species of group PA showed a strong negative correlation with water temperature and a positive correlation with Chl-*a* (Fig. 10b and 10e).

Group PB included two southwest stations (EC17, EC19), and despite the deepening of the water depth, it was distributed in a low-salinity environment. This indicates that the expansion of the CDW also affects the PNC. Compared to groups PA and PC, *Acartia pacifica* showed higher relative abundance in group PB (Fig. 9e). Group PC included three east stations (EC07, EC09, and EC23). Group PC is distributed at the stations where the water temperature was observed to be high in the PNC (Fig. 4b). Group PC showed high zooplankton species diversity compared to groups PA and PB belonging to the PNC, and *Oncaea* spp. *Pseudevadne* spp. were dominant. In the PNC, 18 species, including *Clausocalanus minor*, appeared only in group PC. The indicator species extracted as indicators of group PC showed a positive correlation with water temperature and salinity, and a negative correlation with Chl-*a*.

In the LL, Group LA consisted of 7 stations located in the western part. *Calanus sinicus* showed higher relative abundance at stations EC01, EC03, EC21, and EC23, whereas *Paraclalanus parvus* s. l. was more abundant at the central stations (EC13, EC17, and EC15) (Fig. 9f). Group LA had a broader distribution area with cold water compared to the PNC. The indicator species of Group LA exhibited a negative correlation with water temperature and salinity, but these differences were not statistically significant. On the other hand, Group LC comprised four stations in the eastern part, showing higher zooplankton species diversity and an elevated occurrence rate of *Oncaea* spp. (Fig. 9f). The indicator species of Group LC showed a significant positive correlation with salinity, but the statistical significance could not be confirmed with other environmental factors.

We observed similarities in community structure and water masses among the assemblage groups in different water layers. Groups SA, PA, and LA exhibited similar distributions of dominant species in areas with lower water temperatures. In the SML, these groups had a narrowed distribution, extending to the lowest temperature-affected stations in the PNC, and had a more pronounced influence in the LL. Furthermore, we noticed a trend where the relative abundance of *Calanus sinicus* decreased, whereas the relative abundance of *Paracalanus parvus* s. l. increased. The distribution patterns of Groups SB and PB were also similar, with dominant species occurring in areas with lower salinity. While these groups had a wide distribution in the SML, their distribution narrowed to the stations most affected by salinity in the PNC, and their influence was less evident in the LL. Additionally, we found that the relative abundance of *Acartia pacifica* was higher in areas with lower salinity, and as the abundance of *A. pacifica* decreased, the relative abundance of *P. parvus* s. l. increased, indicating a tendency of replacement in corresponding positions. In the LL layer, no cluster was formed based on the relative abundance of *Acartia pacifica* and *Paracalanus parvus* s. l. This conclusion was drawn by verifying that a low-salinity environment was not as prevalent as observed in the southwest of the SML or PNC, even when considering the horizontal distribution of salinity. In the assemblage groups SC, PC, and LC, characterized by high water temperatures and salinity, we identified a cluster with a high occurrence rate of *Oncaea* spp. and high zooplankton species diversity. These groups, SC, PC, and LC, exhibited a distribution trend predominantly in the eastern part of the surveyed area across all layers.

Shi et al. (2018) proposed the classification of stable zooplankton assemblages in the Yellow Sea and nECS, including the Yellow Sea neritic community, the Yellow Sea central community, the Yellow Sea and East China Sea mixed water community, and the East China Sea Shelf mixed water community. In our study, we aimed to explain the continuity of the community structure for each layer. Based on our findings, we suggest that during periods of significant inflow from the Changjiang River, the zooplankton assemblages form the Yellow Sea and northern East China Sea shelf mixed water community, the CDW and northern East China Sea shelf mixed water community, and the TWC community.

The interaction between different water masses can create favorable conditions for zooplankton to encounter food sources (Morgan et al., 2005). The vertical representation of the abundance of the classified assemblages used in cluster analysis revealed that zooplankton abundance decreased in the groups strongly influenced by the CDW as the sampling sites approached the Changjiang River estuary. In contrast, in layers where the CDW meets with the Yellow Sea cold water, the abundance of zooplankton exhibited an increasing trend (Fig. 11). Additionally, zooplankton abundance decreased in areas strongly affected by the TWW, but it increased in the layers where the Yellow Sea cold water was encountered (Fig. 11). Moreover, in the marine environment of the nECS, phytoplankton biomass is influenced by nutrient-rich substances transported by the CDW (Chen et al., 2009; Chen et al., 2017). Phytoplankton densities were found to be higher in regions with relatively low salinity (Fig. 5g, h). In the SML at Line03, there was a decreasing trend in phytoplankton density as the distance from the Changjiang River estuary increased, with the same trend observed in the CML (Fig. 5g, h). Diatoms were generally dominant in areas influenced by the CDW, with certain species such as *Paralia sulcata, Actinoptychus undulatus*, and *Coscinodiscus radiatus* known to dominate the plankton community of the Changjiang River estuary during summer and play a major role as primary producers in the nECS (Chen et al., 2019). The large inflow of freshwater may reduce competition for food for zooplankton, leading to a temporary decrease in zooplankton abundance and an increase in phytoplankton abundance. In other words, the influx of large amounts of freshwater provides an opportunity for zooplankton abundance to recover. Therefore, future studies should focus on characterizing the progress of zooplankton population recovery in the nECS following a significant influx of CDW.

5. Summary and conclusion

In the nECS, the distribution of water masses during summer is influenced by various factors, such as the Yellow Sea cold water, continental shelf water, CDW, the TWWC, and the TWC. These water mass distributions have a significant impact on the structure of zooplankton assemblages, including species composition, abundance, and diversity. Based on our analysis, we classified the zooplankton assemblages into three groups: the Yellow Sea and continental shelf mixed assemblage, the Changjiang River and continental shelf mixed assemblage, and the TWC assemblage. The inflow of CDW leads to a decrease in salinity, which in turn affects the phytoplankton biomass, zooplankton transport, population dynamics, and species composition in the nECS. Our study revealed the presence of multiple vertically distributed communities at the sampled stations, allowing us to overcome the limitations of vertical collection and gain detailed information on water mass structures through cluster analysis and vertical arrangement of the proposed assemblage groups. This approach provided valuable insights into the vertical structure of water masses and their association with zooplankton communities, thus improving upon previous studies that relied solely on vertical sampling in the nECS.

CRediT authorship contribution statement

Seohwi Choo: . **Myeong-Taek Kwak:** . **Yang-Ki Cho:** . **Yang Ho Yoon:** . **Ho Young Soh:** Funding acquisition.

Declaration of Competing Interest

The authors declare the following financial interests/personal relationships which may be considered as potential competing interests.

Data availability

Data will be made available on request.

Acknowledgements

We thank anonymous reviewers for helping in the revision of the paper. We are grateful to the crew of the T/V Saedongbaek, and Zooplankton Species Diversity Laboratory members at the Chonnam National University for their support in the field. This research was supported by Korea Institute of Marine Science & Technology Promotion (KIMST) funded by the Ministry of Oceans and Fisheries, Korea (20180384). We would also like to thank EssayReview (www. essayreview.co.kr) for the English language editing.

Appendix A. Supplementary data

Supplementary data to this article can be found online at https://doi.org/10.1016/j.ecolind.2023.110847.

References

Cáceres, M.D., Legendre, P., 2009. Associations between species and groups of sites: indices and statistical inference. Ecology 90 (12), 3566–3574. https://doi.org/10.1890/08-1823.1.

Chang, P.H., Isobe, A., 2003. A numerical study on the Changjiang diluted water in the Yellow and East China Seas. J. Geophys. Res.: Oceans. 108 (C9), 3299. https://doi.org/10.1029/2002JC001749.

Chen, C., Beardsley, R.C., Limeburner, R., Kim, K., 1994. Comparison of winter and summer hydrographic observations in the Yellow and East China Seas and adjacent Kuroshio during 1986. Continental Shelf Res. 14 (7–8), 909–929. https://doi.org/10.1016/0278-4343(94)90079-5.

Chen, C.C., Shiah, F.K., Chiang, K.P., Gong, G.C., Kemp, W.M., 2009. Effects of the Changjiang (Yangtze) River discharge on planktonic community respiration in the East China Sea. J. Geophys. Res. Oceans 114 (C3). https://doi.org/10.1029/2008JC004891.

Chen, C.C., Gong, G.C., Chou, W.C., Chung, C.C., Hsieh, C.H., Shiah, F.K., Chiang, K.P., 2017. The influence of episodic flooding on a pelagic ecosystem in the East China Sea. Biogeosciences 14 (10), 2597–2609. https://doi.org/10.5194/bg-14-2597-2017.

Chen, M., Li, Y., Qi, H., Wang, L., Zhang, A., Shen, L., Fang, Q., 2019. The influence of season and Typhoon Morakot on the distribution of diatoms in surface sediments on the inner shelf of the East China Sea. Mar. Micropaleontol. 146, 59–74. https://doi.org/10.1016/j.marmicro.2019.01.003.

Chen, H., Qi, Y., Liu, G., 2011. Spatial and temporal variations of macro-and mesozooplankton community in the Huanghai Sea (Yellow Sea) and East China Sea in summer and winter. Acta Oceanol. Sin. 30 (2), 84–95. https://doi.org/10.1007/s13131-011-0108-5.

Chen, C., Xue, P., Ding, P., Beardsley, R.C., Xu, Q., Mao, X.M., Gao, G., Qi, J., Li, C., Lin, H., Cowles, G., Shi, M., 2008. Physical mechanisms for the offshore detachment of the Changjiang Diluted Water in the East China Sea. J. Geophys. Res. Oceans 113, C02002. https://doi.org/10.1029/2006JC003994.

Cho, Y.K., Seo, G.H., Choi, B.J., Kim, S., Kim, Y.G., Youn, Y.H., Dever, E.P., 2009. Connectivity among straits of the northwest Pacific marginal seas. J. Geophys. Res. Oceans 114 (C6). https://doi.org/10.1029/2008JC005218.

Conceição, L.R.d., Demoner, L.E., Pereira, J.B., Perassoli, F., Ghisolfi, R.D., Bastos, A.C., Junior, C.D., Lázaro, G.C.S., Lemos, K.d.N., Fernandes, L.F.L., 2021. Copepod community structure after a mining dam disaster in the Southwestern Atlantic Ocean. Estuar. Coast. Shelf Sci. 254, 107325.

Cui, T., Chen, X., Zou, X., Zhang, Q., Li, S., Zeng, H., 2022. State of the climate in the Three Gorges Region of the Yangtze River basin in 2020. Atmos. Oceanic Sci. Lett. 15 (2), 100112.

Dufrêne, M., Legendre, P., 1997. Species assemblages and indicator species: the need for a flexible asymmetrical approach. Ecol. Monogr. 67 (3), 345–366. https://doi.org/10.1890/0012-9615(1997)067[0345:SAAIST]2.0.CO;2.

Folt, C.L., Burns, C.W., 1999. Biological drivers of zooplankton patchiness. Trends Ecol. Evol. 14 (8), 300–305. https://doi.org/10.1016/S0169-5347(99)01616-X.

Gao, X., Song, J., Li, X., 2011. Zooplankton spatial and diurnal variations in the Changjiang River estuary before operation of the Three Gorges Dam. Chin. J. Oceanol. Limnol. 29 (3), 591–602. https://doi.org/10.1007/s00343-011-0098-3.

Grieco, L., Tremblay, L.B., Zambianchi, E., 2005. A hybrid approach to transport processes in the Gulf of Naples: an application to phytoplankton and zooplankton population dynamics. Cont. Shelf Res. 25 (5–6), 711–728. https://doi.org/10.1016/j.csr.2004.10.014.

Hays, G.C., Richardson, A.J., Robinson, C., 2005. Climate change and marine plankton. Trends Ecol. Evol. 20 (6), 337–344. https://doi.org/10.1016/j.tree.2005.03.004.

Hickox, R., Belkin, I., Cornillon, P., Shan, Z., 2000. Climatology and seasonal variability of ocean fronts in the East China, Yellow and Bohai Seas from satellite SST data. Geophys. Res. Lett. 27 (18), 2945–2948. https://doi.org/10.1029/1999GL011223.

Hsiao, S.H., Kâ, S., Fang, T.H., Hwang, J.S., 2011. Zooplankton assemblages as indicators of seasonal changes in water masses in the boundary waters between the East China Sea and the Taiwan Strait. Hydrobiologia 666, 317–330. https://doi.org/10.1007/s10750-011-0628-1.

Hur, H.B., Jacobs, G.A., Teague, W.J., 1999. Monthly variations of water masses in the Yellow and East China Seas, November 6, 1998. J. Oceanogr. 55, 171–184. https://doi.org/10.1023/A:1007885828278.

Jang, S.T., Lee, J.H., Kim, C.H., Jang, C.J., Jang, Y.S., 2011. Movement of cold water mass in the northern East China Sea in summer. The Sea 16 (1), 1–13. https://doi.org/10.7850/jkso.2011.16.1.001.

Jeong, Y.S., Choo, S., Soh, H.Y., 2022. Influence of rainfall events on zooplankton community characteristics and feeding habits in estuarine–coastal environments. Front. Mar. Sci. 9 https://doi.org/10.3389/fmars.2022.950695.

Jiang, T., Kundzewicz, Z.W., Su, B., 2008. Changes in monthly precipitation and flood hazard in the Yangtze River Basin, China. Int. J. Climatol. 28 (11), 1471–1481. https://doi.org/10.1002/joc.1635.

Jiang, Z., Liu, J., Chen, J., Chen, Q., Yan, X., Xuan, J., Zeng, J., 2014. Responses of summer phytoplankton community to drastic environmental changes in the Changjiang (Yangtze River) estuary during the past 50 years. Water Res. 54, 1–11. https://doi.org/10.1016/j.watres.2014.01.032.

Kim, S.H., Choi, B.K., Kim, E., 2020. Study on the behavior of the water temperature inversion layer in the northern East China Sea. J. Mar. Sci. Eng. 8 (3), 157. https://doi.org/10.3390/jmse8030157.

Kim, S., Park, J.H., Kug, J.S., 2022. Tropical origins of the record-breaking 2020 summer rainfall extremes in East Asia. Sci. Rep. 12 (1), 1–12. https://doi.org/10.1038/s41598-022-09297-4.

Kimoto, M., 2005. Simulated change of the East Asian circulation under global warming scenario. Geophys. Res. Lett. 32 (16), 1–5. https://doi.org/10.1029/2005GL023383.

Kondo, M., 1985. Oceanographic investigations of fishing grounds in the East China Sea and the Yellow Sea-1. Characteristics of the mean temperature and salinity distributions measured at 50m and near the bottom. Seikai Reg. Fisheries Res. Labor. 62, 19–66.

Landry, M.R., Hood, R.R., Davies, C.H., 2020. Mesozooplankton biomass and temperature-enhanced grazing along a 110° E transect in the eastern Indian Ocean. Mar. Ecol. Prog. Ser. 649, 1–19. https://doi.org/10.3354/meps13444.

Lee, J.Y., Park, W., Moon, S.Y., Cha, H.K., 2019. Distribution and indicator species of zooplankton in the East Sea, Yellow Sea and Northern East China Sea in winter. J. Environ. Biol. 40 (5(SI)), 871–883.

Legendre, P., Legendre, L., 1998. Developments in environmental modelling. Numerical ecology. Elsevier, Kidlington, UK.

Lie, H.J., 1984. A note on water masses and general circulation in the Yellow Sea (Hwanghae). J. Oceanogr. Soc. Korea 19 (2), 187–194.

Lie, H.J., Cho, C.H., 2016. Seasonal circulation patterns of the Yellow and East China Seas derived from satellite-tracked drifter trajectories and hydrographic observations. Prog. Chem. Org. Nat. Prod.in Oceanography. 146, 121–141. https://doi.org/10.1016/j.pocean.2016.06.004.

Liu, Z., Gan, J., Hu, J., Wu, H., Cai, Z., Deng, Y., 2021. Progress on circulation dynamics in the East China Sea and southern Yellow Sea: Origination, pathways, and destinations of shelf currents. Prog. Oceanogr. 193, 102553 https://doi.org/10.1016/j.pocean.2021.102553.

Liu, X., Hu, X., Ao, X., Wu, X., Ouyang, S., 2018. Community characteristics of aquatic organisms and management implications after construction of Shihutang Dam in the Gangjiang River, China. Lake Reservoir Manage. 34 (1), 42–57. https://doi.org/10.1080/10402381.2017.1373716.

Meehl, G.A., Stocker T.F., Collins, W.D., Friedlingstein P., Gaye A.T., Gregory J.M., Kitoh A., Knutti R., Murphy J.M., Noda A., Raper S.C.B., Watterson I.G., Weaver A.J., Zhao Z.C., 2007. Global climate projections. In: Climate change 2007: The physical science basis. Contribution of Working Group I to the Fourth Assessment Report of the Intergovernmental Panel on Climate Change [Solomon, S., D. Qin, M. Manning, Z. Chen, M. Marquis, K.B. Averyt, M. Tignor and H.L. Miller (eds.)]. Cambridge University Press, Cambridge, United Kingdom and New York, NY, USA.

Morgan, C.A., De Robertis, A., Zabel, R.W., 2005. Columbia River plume fronts. I. Hydrography, zooplankton distribution, and community composition. Mar. Ecol. Prog. Ser. 299, 19–31. https://doi.org/10.3354/meps299019.

Nakao, T., 1977. Oceanic variability in relation to fisheries in the East China Sea and the Yellow Sea. J. Faculty Mar. Sci. Technol. Tokai Univ. 199–367.

Park, S., Chu, P., 2008. Characteristics of thermal fine structure in the southern Yellow Sea and the East China Sea from airborne expendable bathythermograph measurements. J. Oceanogr. 64 (6), 859–875. https://doi.org/10.1007/s10872-008-0071-8.

Park, K.W., Oh, H.J., Moon, S.Y., Yoo, M.H., Youn, S.H., 2022. Effects of miniaturization of the summer phytoplankton community on the marine ecosystem in the northern East China Sea. J. Mar. Sci. Eng. 10 (3), 315. https://doi.org/10.3390/jmse10030315.

Seung, Y.H., 1992. Water masses and circulations around Korean Peninsula. J. Oceanol. Soc. Korea 27 (4), 324–331.

Shi, Y.Q., Zuo, T., Yuan, W., Sun, J.Q., Wang, J., 2018. Spatial variation in zooplankton communities in relation to key environmental factors in the Yellow Sea and East

China Sea during winter. Cont. Shelf Res. 170, 33–41. https://doi.org/10.1016/j.csr.2018.10.004.
Shin, S.S., Choi, S.Y., Seo, M.H., Lee, S.J., Soh, H.Y., Youn, S.H., 2022. Spatiotemporal distribution characteristics of copepods in the water masses of the northeastern East China Sea. J. Mar. Sci. Eng. 10 (6), 754. https://doi.org/10.3390/jmse10060754.
Taylor, A.H., Allen, J., Clark, P.A., 2002. Extraction of a weak climatic signal by an ecosystem. Nature 416 (6881), 629–632. https://doi.org/10.1038/416629a.
Tseng, L.C., Souissi, S., Dahms, H.U., Chen, Q.C., Hwang, J.S., 2008. Copepod communities related to water masses in the southwest East China Sea. Helgoland Mar. Res. 62, 153–165. https://doi.org/10.1007/s10152-007-0101-8.
Wang, B., 2006. Cultural eutrophication in the Changjiang (Yangtze River) plume: History and perspective. Estuar. Coast. Shelf Sci. 69 (3–4), 471–477. https://doi.org/10.1016/j.ecss.2006.05.010.
Wang, L.i., Chen, Q., Han, R., Wang, B., Tang, X., 2016. Zooplankton community in Yangtze River Estuary and adjacent sea areas after the impoundment of the Three Gorges Reservoir. Ann. Limnol. - Int. J. Lim. 52, 273–284.
Wang, W., Sun, S., Zhang, F., Sun, X., Zhang, G., 2018. Zooplankton community structure, abundance and biovolume in Jiaozhou Bay and the adjacent coastal Yellow Sea during summers of 2005–2012: relationships with increasing water temperature. J. Oceanol. Limnol. 36 (5), 1655–1670. https://doi.org/10.1007/s00343-018-7099-4.
Wang, R., Zuo, T., Wang, K.E., 2003. The Yellow Sea cold bottom water—an oversummering site for Calanus sinicus (Copepoda, Crustacea). J. Plankton Res. 25 (2), 169–183. https://doi.org/10.1093/plankt/25.2.169.
Wiebe, P.H., Morton, A.W., Bradley, A.M., Backus, R.H., Craddock, J.E., Barber, V., Cowles, T.J., Flierl, G.R., 1985. New development in the MOCNESS, an apparatus for sampling zooplankton and micronekton. Mar. Biol. 87 (3), 313–323.
WoRMS Editorial Board (2023). World Register of Marine Species. Available from https://www.marinespecies.org at VLIZ. Accessed 2023-08-08. doi: 10.14284/170.
Wu, J., Huang, J., Han, X., Xie, Z., Gao, X., 2003. Three-Gorges Dam—experiment in habitat fragmentation? Science 300 (5623), 1239–1240. https://doi.org/10.1126/science.1083312.
Zhang, C.I., Seo, Y.I., Kang, H.J., Lim, J.H., 2019. Exploitable carrying capacity and potential biomass yield of sectors in the East China Sea, Yellow Sea, and East Sea/Sea of Japan large marine ecosystems. Deep Sea Res., Part II 163, 16–28. https://doi.org/10.1016/j.dsr2.2018.11.016.